Computer Aided Geometric Design 35–36 (2015) 121–136

Contents lists available at ScienceDirect

Computer Aided Geometric Design

www.elsevier.com/locate/cagd

Nitsche method for isogeometric analysis of Reissner–Mindlin plate with non-conforming multi-patches

Xiaoxiao Du [a,b], Gang Zhao [a], Wei Wang [a,*]

[a] School of Mechanical Engineering and Automation, Beihang University, Beijing 100191, PR China
[b] School of Mechanical and Automotive Engineering, Hefei University of Technology, Hefei 230009, PR China

ARTICLE INFO

Article history:
Received 20 February 2015
Accepted 11 March 2015
Available online 24 March 2015

Keywords:
Nitsche method
Isogeometric analysis
Reissner–Mindlin plate
Non-conforming

ABSTRACT

Nitsche method application in non-conforming plate is presented in the context of isogeometric analysis. Reissner–Mindlin plate theory is employed to build governing equation and stiffness matrix. We use this theory to solve the elasticity problems of various classical plate models, and compare the obtained results to those from single-patch models and the exact solutions in Kirchhoff theory. The solutions of problem involving the use of complex model are as well obtained using the same Reissner–Mindlin theory and compared to the results from finite element method. All models are built with NURBS (non-uniform rational B-spline) patches with non-conforming mesh along the common boundaries. The algorithms of knot insertion and order elevation are applied to enrich the basis functions of NURBS patches. The results of numerical examples show the accuracy, robustness and high convergence rate of this method.

1. Introduction

Isogeometric Analysis (IGA) proposed by Hughes et al. (2005) achieves true sense of seamless combination of Computer-Aided Design (CAD) and Finite Element Analysis (FEA) with the concept that both the geometry description in design and field variables approximation in analysis use the same NURBS basis functions. More accurate results, less time consumption and other various advantages can be obtained compared with the classical finite element method, so isogeometric analysis won a broad attention as soon as it was proposed. By far, isogeometric analysis has been successfully used in many areas including structural mechanics and vibration (Cottrell et al., 2007, 2006), fluid structure and turbulence (Bazilevs et al., 2006, 2008), plate and shell (Beirão da Veiga et al., 2012; Kiendl et al., 2009), large deformation (Benson et al., 2011), electromagnetics (Buffa et al., 2010), phase-field analysis (Gómez et al., 2008) and so on.

As the unifying mathematical expression of the elementary analytic geometries and free-form shapes, NURBS possesses many fast, efficient and numerically stable algorithms (Piegl and Tiller, 1997). Therefore, it becomes the method most widely used in engineering design and the unique computational geometry technology in prevailing CAD systems as well as the de facto international standards for geometry data exchange. It has a variety of useful mathematical properties such as affine covariance, variation diminishing, and convex hull properties. Additionally, NURBS is equipped with effective algorithms like knot insertion and order elevation, which can be used for the refinement of analysis models without changing the

* Corresponding author. Tel.: +86 10 82338292.
E-mail address: jrrt@buaa.edu.cn (W. Wang).

http://dx.doi.org/10.1016/j.cagd.2015.03.005
0167-8396/

geometric structure. However, the tensor product structure of NURBS based isogeometric analysis has its essential weakness.

The first limitation is that it is impossible to implement the local refinement without propagating superfluous control points. This shortcoming can be overcome by T-spline proposed by Sederberg et al. (2003), which allows the existence of T-junction and makes it possible to build a watertight model with single patch (Sederberg et al., 2008). To some extent, T-spline is the generalization of the NURBS. PHT-spline (Deng et al., 2008) and LR-spline (Dokken et al., 2013) can also be used to realize the local refinement. Moreover, it is difficult to represent a complex geometry with single NURBS patch. This leads to another limitation of NURBS-based isogeometric analysis, which means that various difficulties such as continuity and compatibility problems should be settled between patches when using multiple patches to describe the complex object. Conforming mesh is required to be generated when geometry is built with multi-patches in isogeometric method. While how to deal with non-conforming multi-patch geometries for applications in isogeometric analysis in order to reduce the tedious work involved in coupling the boundaries is still a challenging problem.

Mortar, Penalty and Nitsche are currently existing methods usually employed to solve the non-conforming problems. In mortar method, the extra unknowns are introduced to establish the relationship between different domains along the interfaces, which is one of Lagrange multiplier method essentially (Lacour and Maday, 1997; Moro et al., 2014). It destroys the positive definiteness of matrix in discrete system of equation and makes the solution complex. In penalty method, penalty term is substituted for Lagrange multiplier term to avoid solving a mixed variational formulation. The size of equation system is kept effectively in this method, but the equation set becomes ill-conditioned and the results are sensitive to the value of penalty operator (Toselli and Widlund, 2005; Zhu et al., 2005). Nitsche method is considered to be deduced from mortar and penalty method. It is used to weakly impose Dirichlet boundary conditions originally proposed in Nitsche (1971). This method not only keeps the size of equation system unchanged but also maintains the positive definiteness of matrix (Sanders et al., 2012). Similarly to Nitsche method's application in non-conforming problems, discontinuous Galerkin (DG) method allows for discontinuities in problem unknowns' field (Cockburn et al., 2000). It is successfully applied to various problems such as plates (Marini, 2008), shells (Noels and Radovitzky, 2008), and multi-domains (Mergheim et al., 2004). Furthermore it is used to solve elliptic problems combined with isogeometric method (Brunero et al., 2012). In the context of IGA, Hesch and Betsch used mortar method to handle non-conforming problems in the framework of nonlinear elasticity (Hesch and Betsch, 2012). Embar et al. weakly imposed Dirichlet boundary conditions with Nitsche method and applied it to second- and fourth-order problems (Embar et al., 2010). Nguyen et al. employed Nitsche method to couple two and three dimensional NURBS patches (Nguyen et al., 2014). Apostolatos et al. made the comparison of these methods applied on the two dimensional problems of linear elasticity and eigenfrequency analysis (Apostolatos et al., 2014). Guo and Ruess applied Nitsche method on gluing thin shell structures (Guo and Ruess, 2015). In this paper, the isogeometric analysis of non-conforming plates are investigated with Nitsche method.

Kirchhoff hypothesis and Reissner–Mindlin hypothesis are two widely used theories of plate in finite element method (Zienkiewicz and Taylor, 2005), which deal with thin and thick plate respectively. Both theories were successfully applied to IGA (Beirão da Veiga et al., 2012; Shojaee and Valizadeh, 2012). In contrast with Kirchhoff hypothesis, any cross section of undeformed plate is assumed to remain straight but not perpendicular to the middle surface during the deformation in the assumption of Reissner–Mindlin plates, of which the main features include that shear deformation of plate is considered and basic variables (deflection and rotations) are independently interpolated. It can be used to analyze both thin and thick plate problems and only C^0 continuity should be satisfied across the inner-elements (Quek and Liu, 2003). The principal limitation of this theory, the shear locking phenomenon in thin plates, can be completely precluded with a reformulated version of Reissner–Mindlin theory combining smooth NURBS basis functions (Beirão da Veiga et al., 2015), as well as effectively alleviated by a stabilization approach in IGA (Thai et al., 2012). Moreover, transverse shear deformation should not be neglected for many practical situations. The Mindlin theory, thus is used to study the plate problems in this work.

This paper is organized as follows. Section 2 introduces the problem description and governing equations. Nitsche-type formulation is simply derived in Section 3. Section 4 describes the NURBS basis function and its derivatives. Section 5 discusses the discretization and derives the stiffness matrix based on Mindlin plate theory. Some numerical examples are provided in Section 6.

2. Problem description

Consider the Reissner–Mindlin plate problems in elastic analysis. As depicted in Fig. 1, we define the domain Ω in 3D *Euclidean* space with boundary $\Gamma = \partial\Omega$, which is divided into two non-overlapping bodies by one internal boundary Γ_*. Boundary in each body $\Omega^m (m = 1, 2)$ excluding Γ_* is split into Dirichlet part Γ_u^m and Neumann part Γ_t^m. The prescribed traction $\bar{t}^m$ is posted along its boundary Γ_t^m, and the $\mathbf{n}^m$ defined on the internal boundary Γ_* represents the outward unit normal to corresponding part. The superscript m is used to denote different region Ω^m that is valid, with $m = 1, 2$.

A system of linear elastostatic governing equations of Reissner–Mindlin plate with primary unknown displacement $\mathbf{u}^m$, can be written as

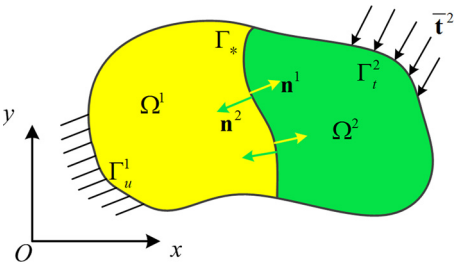

Fig. 1. Computational domain with two bodies.

$$\nabla\boldsymbol{\sigma}^m = -\mathbf{b}^m \qquad in\ \Omega^m \tag{1a}$$

$$\mathbf{u}^m = \bar{\mathbf{u}}^m \qquad on\ \Gamma_u^m \tag{1b}$$

$$\boldsymbol{\sigma}^m \cdot \mathbf{n}^m = \bar{\mathbf{t}}^m \qquad on\ \Gamma_t^m \tag{1c}$$

$$\mathbf{u}^1 = \mathbf{u}^2 \qquad on\ \Gamma_* \tag{1d}$$

$$\boldsymbol{\sigma}^1 \cdot \mathbf{n}^1 = -\boldsymbol{\sigma}^2 \cdot \mathbf{n}^2 \qquad on\ \Gamma_* \tag{1e}$$

where $\boldsymbol{\sigma}$ and $\bar{\mathbf{u}}$ are the stress tensor and prescribed displacement, respectively. According to the plate theory, the displacement $\mathbf{u}$ is defined as

$$\mathbf{u} = \begin{Bmatrix} u \\ v \\ w \end{Bmatrix} = \begin{Bmatrix} z\theta_y \\ -z\theta_x \\ w \end{Bmatrix} \tag{2}$$

in which u, v, w are the displacements along the three coordinate axes, θ_x and θ_y are the rotation angles about X-axis and Y-axis.

Then the strain is given by Zhu et al. (2005):

$$\boldsymbol{\epsilon}^m(\mathbf{u}) = 0.5(\nabla\mathbf{u}^m + \nabla^T\mathbf{u}^m) \tag{3}$$

and the stress can be written as

$$\boldsymbol{\sigma}^m(\mathbf{u}) = \mathbf{C}^m : \boldsymbol{\epsilon}^m(\mathbf{u}) \tag{4}$$

where $\mathbf{C}^m$ is elastic matrix depending on material properties. We assume that both computational domains have the same linear isotropic elastic materials in the context.

3. Weak form of Nitsche-type method

We simply derive the weak form of Nitsche-type formulation in this section.

Let us denote the solution space and weighting space by $\mathcal{S}^m$ and $\mathcal{V}^m$ over the domain Ω^m, respectively. Each $\mathbf{u}^m \in \mathcal{S}^m$ satisfies the condition $\mathbf{u}^m = \bar{\mathbf{u}}^m$ on Dirichlet boundary Γ_u^m, and each $\mathbf{w}^m \in \mathcal{V}^m$ satisfies $\mathbf{w}^m = \mathbf{0}$ on Γ_u^m, which can be rewritten as

$$\mathcal{S}^m = \{\mathbf{u}^m(x) | \mathbf{u}^m(x) \in H^1(\Omega^m), \mathbf{u}^m = \bar{\mathbf{u}}^m, on\ \Gamma_u^m\}$$

$$\mathcal{V}^m = \{\mathbf{w}^m(x) | \mathbf{w}^m(x) \in H^1(\Omega^m), \mathbf{w}^m = \mathbf{0}, on\ \Gamma_u^m\}$$

In each domain Ω^m, the variational form of the boundary value problem given by Eqs. (1a)–(1e) is: Find $\mathbf{u}^m \in \mathcal{S}^m$ such that for all $\mathbf{w}^m \in \mathcal{V}^m$

$$a(\mathbf{u}^m, \mathbf{w}^m) = L(\mathbf{w}^m) \tag{5}$$

where bilinear form $a(\cdot,\cdot)$ and linear form $L(\cdot)$ are defined as follows (Cottrell et al., 2009):

$$a(\mathbf{u}^m, \mathbf{w}^m) = \int_{\Omega^m} \boldsymbol{\epsilon}^m(\mathbf{w}) : \boldsymbol{\sigma}^m \tag{6a}$$

$$L(\mathbf{w}^m) = \int_{\Omega^m} \mathbf{w}^m \cdot \mathbf{b}^m + \int_{\Gamma_t^m} \mathbf{w}^m \cdot \bar{\mathbf{t}}^m \tag{6b}$$

Here the variational form of Eq. (5) is called a weak form compared with the strong form of Eq. (1).

Considering the coupling of solutions of two bodies, extra constraint terms are required to eliminate the limitation of non-matching situation between two domains along the interface Γ_*. Several methods were proposed to solve this problem, such as Lagrange multiplier, penalty, and Nitsche method as introduced in Section 1. In the approach of Lagrange multiplier, the so-called Lagrange multiplier field interpreted as the traction field is introduced to be added to the variational formulation. However, this operation compels us to settle a mixed variational formulation containing two fields, displacement and traction. Penalty approach is one of the methods that can avoid this disadvantage, which employs a penalty parameter multiplying the jump operator on the interface to solve the unique unknown field: displacement. Unfortunately, penalty method is variationally inconsistent and the solutions are sensitive to the penalty parameter. Nitsche method provides a new weak constraint enforcement to resolve these problems. For the two-body problem described in Section 2, the standard application of Nitsche method is: Find $\mathbf{u}^1, \mathbf{u}^2 \in \mathcal{S}^1 \times \mathcal{S}^2$ such that

$$\sum_{m=1}^{2} \int_{\Omega^m} \boldsymbol{\epsilon}^m(\mathbf{w}) : \boldsymbol{\sigma}^m d\Omega - \int_{\Gamma_*} (\llbracket \mathbf{w} \rrbracket \otimes \mathbf{n}^1) : \langle \boldsymbol{\sigma} \rangle d\Gamma - \int_{\Gamma_*} (\llbracket \mathbf{u} \rrbracket \otimes \mathbf{n}^1) : \langle \boldsymbol{\sigma}(\mathbf{w}) \rangle d\Gamma + \beta \int_{\Gamma_*} \llbracket \mathbf{u} \rrbracket \cdot \llbracket \mathbf{w} \rrbracket d\Gamma$$
$$= \sum_{m=1}^{2} \int_{\Omega^m} \mathbf{w}^m \cdot \mathbf{b}^m d\Omega + \sum_{m=1}^{2} \int_{\Gamma_t^m} \mathbf{w}^m \cdot \bar{\mathbf{t}}^m d\Gamma \tag{7}$$

for all $(\mathbf{w}^1, \mathbf{w}^2) \in \mathcal{V}^1 \times \mathcal{V}^2$. More details can be found in Nguyen et al. (2014), Sanders et al. (2012). Here the double square brackets $\llbracket \cdot \rrbracket$ and angle brackets $\langle \cdot \rangle$ denote jump and average operators, respectively, and defined as:

$$\llbracket \mathbf{u} \rrbracket = \mathbf{u}^1 - \mathbf{u}^2 \tag{8}$$
$$\langle \boldsymbol{\sigma} \rangle = \gamma \boldsymbol{\sigma}^1 + (1-\gamma)\boldsymbol{\sigma}^2 \tag{9}$$

where the parameter γ acts as a weight corresponding to each problem domain and $\gamma \in [0,1]$. $\gamma = 0.5$ is chosen for our study because the same material is used in each domain. Parameter β here has the same form as in penalty method but means differently. It is viewed as the stabilization parameter and plays an important role in the coercivity of bilinear form in Nitsche method (Annavarapu et al., 2012; Dolbow and Harari, 2009).

4. NURBS functions and derivatives

In this section, non-uniform rational B-spline functions and its derivatives are briefly reviewed. We refer readers to Piegl and Tiller (1997) for more details on NURBS.

A knot vector is a series of non-decreasing coordinates in the parameter space, written as $\Xi = \{\xi_1, \xi_2, \cdots, \xi_{n+p+1}\}$, where ξ_i is the ith knot, p denotes the polynomial degree of B-spline basis functions, and n is the number of control points. In this paper, we will only consider open knot vectors in which the first and last knot have $p+1$ multiplicities. Open knot vectors are standard in the CAD literature. B-spline basis functions are interpolatory at both ends of the parameter domain if its knot vectors are open.

With a given knot vector, the B-spline basis functions are defined by Cox–de Boor recursive formula:

$$N_{i,0}(\xi) = \begin{cases} 1 & \text{if } \xi_i \le \xi \le \xi_{i+1} \\ 0 & \text{otherwise} \end{cases} \tag{10}$$

for the beginning with $p = 0$ and

$$N_{i,p}(\xi) = \frac{\xi - \xi_i}{\xi_{i+p} - \xi_i} N_{i,p-1}(\xi) + \frac{\xi_{i+p+1} - \xi}{\xi_{i+p+1} - \xi_{i+1}} N_{i+1,p-1}(\xi) \tag{11}$$

for $p = 1, 2, 3, \cdots$.

Some important properties of B-spline basis functions can be listed as:

(1) Partition of unity: $\sum_{i=1}^{n} N_{i,p}(\xi) = 1$, $\forall \xi$.
(2) Non-negativity: $N_{i,p}(\xi) \ge 0$, $\forall \xi$.
(3) Local support: $N_{i,p}(\xi) > 0$, $\forall \xi \in (\xi_i, \xi_{i+p+1})$.
(4) Differentiability: the B-spline basis are C^∞ continuous in knot intervals and C^{p-k} continuous at a knot ξ_i, where k is the multiplicity of the knot ξ_i in the knot vector.

A sequence of B-spline basis functions of cubic basis is shown in Fig. 2 for an open knot vector $\Xi = \{0, 0, 0, 0, 0.25, 0.5, 0.5, 0.75, 1, 1, 1, 1\}$. The basis functions are interpolatory at two ends of the parameter space, and $C^{p-k} = C^1$ continuous at the knot value $\xi = 0.5$ with the multiplicity $k = 2$.

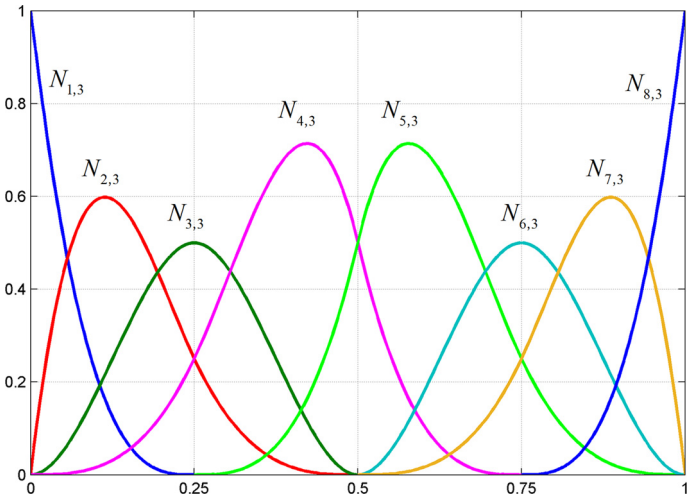

Fig. 2. Cubic basis functions for an open knot vector $\Xi = \{0, 0, 0, 0, 0.25, 0.5, 0.5, 0.75, 1, 1, 1, 1\}$.

The NURBS curve of order p is defined as follows:

$$\mathbf{C}(\xi) = \sum_{i=1}^{n} R_{i,p}(\xi)\mathbf{P}_i \tag{12a}$$

$$R_{i,p}(\xi) = \frac{N_{i,p}(\xi)}{\sum_{j=1}^{n} N_{j,p}(\xi) w_j} \tag{12b}$$

where $\{R_{i,p}\}$ $(i = 1, 2, \cdots, n)$ represent the basis functions of NURBS and the shape functions in IGA, $\{\mathbf{P}_i\}$ are the control points, and $\{w_i\}$ are the weights corresponding to each control point.

Let $\Xi_1 = \{\xi_1, \xi_2, \cdots, \xi_{n+p+1}\}$ and $\Xi_2 = \{\eta_1, \eta_2, \cdots, \eta_{m+q+1}\}$ be the two knot vectors, the NURBS surface is given by

$$\mathbf{S}(\xi, \eta) = \sum_{i=1}^{n}\sum_{j=1}^{m} R_{i,j}^{p,q}(\xi, \eta)\mathbf{P}_{i,j} \tag{13a}$$

$$R_{i,j}^{p,q}(\xi, \eta) = \frac{N_{i,p}(\xi) M_{j,q}(\eta) w_{i,j}}{\sum_{k=1}^{n}\sum_{l=1}^{m} N_{k,p}(\xi) M_{l,q}(\eta) w_{k,l}} \tag{13b}$$

where $\{R_{i,j}^{p,q}\}$ are the basis functions of surface, $\{\mathbf{P}_{i,j}\}$ are the control points emerging as a grid of topologically rectangular array, $\{w_{i,j}\}$ are the corresponding weights, $\{N_{i,p}\}$ and $\{M_{j,q}\}$ are the B-spline basis functions defined on Ξ_1 with order $p+1$ and Ξ_2 with order $q+1$, respectively.

Let R denote the NURBS basis functions, X and W represent the numerators and denominators of the basis respectively, then the basis function can be expressed as

$$R = \frac{X}{W} \Rightarrow RW = X \tag{14}$$

Employing *Leibnitz's* formula, we obtain the nth-order derivatives

$$R' = \frac{X' - RW'}{W} \tag{15a}$$

$$R'' = \frac{X'' - 2R'W' - RW''}{W} \tag{15b}$$

$$R^{(n)} = \frac{X^{(n)} - \sum_{k=1}^{n} \binom{n}{k} R^{(n-k)} W^{(k)}}{W} \tag{15c}$$

where $\binom{n}{k}$ is the binomial coefficient, $(\cdot)$ represents the order of functions.

5. Discretization

In this section, we discretize the non-overlapping problem domains Ω^1 and Ω^2, and derive the stiffness matrix of Mindlin plate employing Nitsche method discussed in previous sections. In the context of isogeometric analysis, the discretization of the approximation functions $u^h \in \mathcal{S}$ and the weighting functions $w^h \in \mathcal{V}$ are defined with the *Galerkin* method as follows:

$$u^h(\mathbf{x}) = \sum_{i=1}^{nel} R_i(\boldsymbol{\xi}) u_i \tag{16}$$

$$w^h(\mathbf{x}) = \sum_{i=1}^{nel} R_i(\boldsymbol{\xi}) w_i \tag{17}$$

in which $\{R_i\}$ represent the NURBS basis functions, *nel* is the number of basis functions in each element of IGA, and $\boldsymbol{\xi}$ denotes the coordinates in geometry parameter domain. Upon substituting Eqs. (16) and (17) into the variational formulation (7), the discrete system equation of Nitsche method is obtained straightforwardly as follow:

$$\begin{bmatrix} \mathbf{K}_b^1 + \mathbf{K}_n^1 + \mathbf{K}_s^1 & \mathbf{K}_c \\ \mathbf{K}_c^T & \mathbf{K}_b^2 + \mathbf{K}_n^2 + \mathbf{K}_s^2 \end{bmatrix} \begin{Bmatrix} \mathbf{u}^1 \\ \mathbf{u}^2 \end{Bmatrix} = \begin{Bmatrix} \mathbf{F}^1 \\ \mathbf{F}^2 \end{Bmatrix} \tag{18}$$

where $\mathbf{K}_b^m$ denotes the bulk stiffness matrix, $\mathbf{K}_n^m, \mathbf{K}_s^m$ and $\mathbf{K}_c$ denote the Nitsche contribution term, stabilization term and coupling matrix, respectively. The detailed derivation is recommended to Annavarapu et al. (2012). For simplification, Eq. (18) can be rewritten as $\mathbf{Ku} = \mathbf{F}$ with the same form in the classical finite element method.

The bulk stiffness matrix is given by:

$$\mathbf{K}_b^m = \int_{\Omega^m} (\mathbf{B}^m)^T \mathbf{C}^m \mathbf{B}^m d\Omega \tag{19}$$

where $\mathbf{B}^m$ is the gradient of the shape functions. The matrix derived from Nitsche contribution term can be defined as:

$$\mathbf{K}_n^m = -\frac{1}{2}\int_{\Gamma_*} (\mathbf{R}^m)^T \mathbf{n}\mathbf{C}^m \mathbf{B}^m d\Gamma - \frac{1}{2}\int_{\Gamma_*} (\mathbf{B}^m)^T (\mathbf{C}^m)^T \mathbf{n}^T \mathbf{R}^m d\Gamma \tag{20}$$

The stabilization term $\mathbf{K}_s^m$ is expressed as:

$$\mathbf{K}_s^m = \beta \int_{\Gamma_*} (\mathbf{R}^m)^T \mathbf{R}^m d\Gamma \tag{21}$$

and the coupling matrix can be written as:

$$\mathbf{K}_c = -\beta \int_{\Gamma_*} (\mathbf{R}^1)^T \mathbf{R}^2 d\Gamma - \frac{1}{2}\int_{\Gamma_*} (\mathbf{R}^1)^T \mathbf{n}\mathbf{C}^2 \mathbf{B}^2 d\Gamma + \frac{1}{2}\int_{\Gamma_*} (\mathbf{B}^1)^T (\mathbf{C}^1)^T \mathbf{n}^T \mathbf{R}^2 d\Gamma \tag{22}$$

in which superscript $m = 1, 2$ and weighting parameter $\gamma = 0.5$ are applied on all of the above four discrete equations. The value of stabilization parameter β should guarantee the coercivity of bilinear form defined in Eq. (7). Assuming that there exists a mesh-dependent constant $C_0 > 0$ such that

$$\| \nabla w^h \cdot \mathbf{n} \|_{\Gamma_*} \leq C_0 (w^h, w^h)^{\frac{1}{2}} \tag{23}$$

The stabilization parameter should satisfy the inequation: $\beta \geq C_0^2$ and the suitable value $\beta = 2C_0^2$ is recommended to use from Dolbow and Harari (2009), Embar et al. (2010). $(\cdot)$ denotes L_2 inner product, expressing an energy norm.

In the theory of Reissner–Mindlin plate, the transverse displacement w and two rotation angles θ_x, θ_y are three independent variables. Only the deformation in middle surface of plate is considered here. Therefore, we employ w, θ_x, θ_y to serve as the components of displacement field $\mathbf{u}$, which is written as:

$$\mathbf{u} = [\, w \quad \theta_x \quad \theta_y \,]^T \tag{24}$$

Under isogeometric framework, NURBS basis function in geometry is introduced to be used as shape function in FEA, and the relationship is obtained between the basis functions and control variables. Then the displacement fields in each element can be expressed as:

$$\mathbf{u}^e = \begin{Bmatrix} w \\ \theta_x \\ \theta_y \end{Bmatrix} = \sum_{i=1}^{nel} \begin{bmatrix} R_i & 0 & 0 \\ 0 & R_i & 0 \\ 0 & 0 & R_i \end{bmatrix} \begin{Bmatrix} w_i \\ \theta_{xi} \\ \theta_{yi} \end{Bmatrix} = \mathbf{R}^e \boldsymbol{\delta}^e \tag{25}$$

where $\mathbf{R}$ is the shape function matrix, $\boldsymbol{\delta}^e$ denotes the control variables at the position of corresponding control points and superscript e indicates the relevant element. In contrast to the interpolatory shape functions in conventional finite element analysis, NURBS basis function is commonly non-interpolatory, which will produce some difficulties on the imposition of essential boundary conditions on certain circumstance. It is shown that boundary collocation method, Nitsche variational method and Lagrange multiplier method can be used to enforce the essential boundary conditions from Embar et al. (2010), Shojaee and Valizadeh (2012), Wang and Xuan (2010).

The pseudo-strain of the plate is then given by

$$\begin{aligned}\boldsymbol{\epsilon}_p^e &= \left\{ \frac{\partial \theta_y}{\partial x} \quad -\frac{\partial \theta_x}{\partial y} \quad \frac{\partial \theta_y}{\partial y} - \frac{\partial \theta_x}{\partial x} \quad \theta_x - \frac{\partial w}{\partial y} \quad \theta_y + \frac{\partial w}{\partial x} \right\}^T \\ &= \sum_{i=1}^{nel} \begin{bmatrix} 0 & 0 & R_{i,x} \\ 0 & -R_{i,y} & 0 \\ 0 & -R_{i,x} & R_{i,y} \\ -R_{i,y} & R_i & 0 \\ R_{i,x} & 0 & R_i \end{bmatrix} \begin{Bmatrix} w_i \\ \theta_{xi} \\ \theta_{yi} \end{Bmatrix} \\ &= \mathbf{B}^e \boldsymbol{\delta}^e \end{aligned} \tag{26}$$

The pseudo-stress is defined as

$$\begin{aligned}\boldsymbol{\sigma}_p^e &= \{ M_x \quad M_y \quad M_{xy} \quad Q_y \quad Q_x \}^T \\ &= \begin{Bmatrix} \mathbf{D}_b & \mathbf{0} \\ \mathbf{0} & \mathbf{D}_s \end{Bmatrix} \boldsymbol{\epsilon}_p^e \\ &= \mathbf{B}^e \mathbf{C} \boldsymbol{\delta}^e \end{aligned} \tag{27}$$

where $M_{(\cdot)}$, $Q_{(\cdot)}$ are plate bending moments and shear forces, $\mathbf{D}_b, \mathbf{D}_s$ are bending constitutive matrix and shear constitutive matrix defined as:

$$\mathbf{D}_b = D_0 \begin{bmatrix} 1 & \nu & 0 \\ \nu & 1 & 0 \\ 0 & 0 & \dfrac{1-\nu}{2} \end{bmatrix} \tag{28}$$

$$\mathbf{D}_s = \frac{Et}{2(1+\nu)\lambda} \begin{bmatrix} 1 & 0 \\ 0 & 1 \end{bmatrix} \tag{29}$$

where E, t, ν are Young's modulus, thickness of the plate and Poisson ratio, respectively, $D_0 = \frac{Et^3}{12(1-\nu^2)}$ is the flexural rigidity of the plate, λ is shear correction factor chosen as $\lambda = 6/5$ (Quek and Liu, 2003). The outward unit normal $\mathbf{n}$ is given by:

$$\mathbf{n} = \begin{bmatrix} n_x & 0 & n_y & 0 & n_z \\ 0 & n_y & n_x & n_z & 0 \\ 0 & 0 & 0 & n_y & n_x \end{bmatrix} \tag{30}$$

Then, the stiffness matrices in Eqs. (19)–(22) can be calculated with shape function $\mathbf{R}$, pseudo-strain matrix $\boldsymbol{\epsilon}$, pseudo-stress $\boldsymbol{\sigma}$ and outward unit normal $\mathbf{n}$.

6. Numerical examples

We consider several numerical examples of Reissner–Mindlin multi-patch plates with different boundary conditions and show that Nitsche method gives good results in the analysis of non-conforming situations. For the sake of comparison, Mindlin theory is employed to analyze classical thin plate built with non-conforming multi-patch and single patch, and the results are compared to the analytical solutions obtained under the theory of Kirchhoff. Meanwhile, we study the problems of a complex cantilever plate model and compare the results with that of finite element method. The methods of knot insertion and order elevation are used to enrich the basis of NURBS model to explore the convergence, which have much in common with the *h*-refinement strategy and *p*-refinement strategy in classical finite element analysis, respectively. *Gauss* quadrature rule is applied to compute all integral terms. Some other quadrature rules for isogeometric analysis are introduced in Auricchio et al. (2012), Hughes et al. (2010), Schillinger et al. (2014). The material properties Young's modulus $E = 2.0 \times 10^8$ N/m^2, Poisson ratio $\nu = 0.3$ are taken to all examples unless special instructions. We denote patch 1 for left patch and patch 2 for right patch while the models are built with two patches in the following examples. The q-direction of NURBS patch is defined along the common boundary and another direction is called p-direction.

6.1. Simply supported square plate subjected to uniform load

We start with an example of simply supported square plate of side a subjected to uniformly distributed load $p(x, y) = q_0$. The transverse displacement and bending moments are investigated in this section. The x axis is coincided with the axis of symmetry of the plate and y axis is fixed on the left side of square plate as shown in Fig. 3(a). Here we assume that $a = 1$ m, thickness $t = 0.01$ m and uniform pressure $q_0 = -100$ N. The exact solutions in terms of deflection can be denoted by Ventsel and Krauthammer (2001):

$$w = \frac{4q_0 a^4}{\pi^5 D_0} \sum_m^{\infty} \frac{1}{m^5} \left(1 - \frac{\alpha_m \tanh \alpha_m + 2}{2 \cosh \alpha_m} \cosh \frac{2\alpha_m y}{a} + \frac{\alpha_m}{2 \cosh \alpha_m} \frac{2y}{a} \sinh \frac{2\alpha_m y}{a} \right) \sin \frac{m\pi x}{a} \tag{31}$$

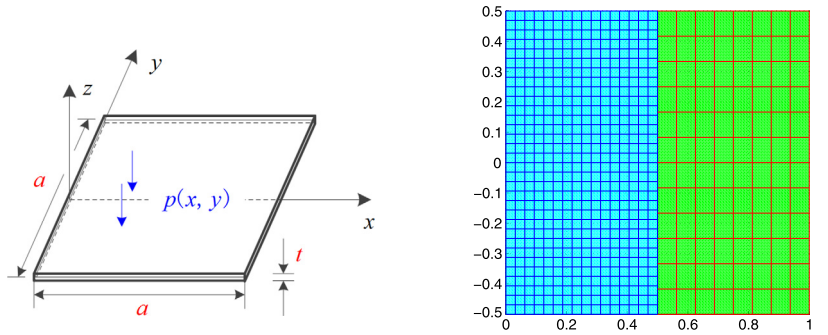

(a) The dimensions of square plate (b) Non-conforming mesh for the plate

Fig. 3. Simply supported square plate under uniform load. (a) The dimensions of square plate and (b) the refinement of plate.

and the exact bending moments are

$$M_x = \frac{q_0 x(a-x)}{2} + (1-\nu) q_0 a^2 \pi^2 \sum_m^{\infty} m^2 \left[B_m \cosh\frac{m\pi y}{a} + C_m \left(\frac{m\pi y}{a} \sinh\frac{m\pi y}{a} - \frac{2\nu}{1-\nu} \cosh\frac{m\pi y}{a} \right) \right] \times \sinh\frac{m\pi y}{a} \tag{32}$$

$$M_y = \nu \frac{q_0 x(a-x)}{2} - (1-\nu) q_0 a^2 \pi^2 \sum_m^{\infty} m^2 \left[B_m \cosh\frac{m\pi y}{a} + C_m \left(\frac{m\pi y}{a} \sinh\frac{m\pi y}{a} + \frac{2}{1-\nu} \cosh\frac{m\pi y}{a} \right) \right] \times \sinh\frac{m\pi y}{a} \tag{33}$$

where $\alpha_m = \frac{m\pi}{2}$, $m = 1, 2, 3, \ldots$, B_m and C_m are given as

$$B_m = -\frac{2q_0 a^4 (\alpha_m \sinh\alpha_m + 2\cosh\alpha_m)}{\pi^5 m^5 D_0 \cosh^2\alpha_m}$$

$$C_m = \frac{2q_0 a^4}{\pi^5 m^5 D_0 \cosh\alpha_m}$$

We build the square plate with two patches which are discretized by non-conforming mesh: 16×32 elements and polynomial degrees $p_1 = 3$, $q_1 = 4$ for left patch, 8×12 elements and polynomial degrees $p_2 = 4$, $q_2 = 3$ for right patch, see Fig. 3(b). Two domains Ω^1, Ω^2 and interface Γ_* can be expressed in physical coordinate system as $\Omega^1 = \{0 \le x < a/2, -a/2 \le y \le a/2\}$, $\Omega^2 = \{a/2 < x \le a, -a/2 \le y \le a/2\}$ and $\Gamma_* = \{x = a/2, -a/2 \le y \le a/2\}$. The square plate constructed with single NURBS patch is also explored to do the comparison with a special discretization, 16×16 elements and bicubic polynomial degrees, which is also applied to the next two examples. The deflection w and bending moments M_x and M_y on two domains are plotted under this circumstances in Figs. 4(a), 5(a) and 6(a), from which we can find that all the three variables reach a maximum in the center of square plate. We additionally study the distribution of each control variable along the lines of $y = 0$ and $y = 0.25a$, then compare them with the results obtained from single patch and the exact solutions in Ventsel and Krauthammer (2001). The comparisons in Figs. 4(b), 5(b) and 6(b) show that isogeometric analysis based on Nitsche method has a good approximation on two domains and along the interface. The variables are continuous across the interface according to the colors on opposite sides in post-processing figures.

What's more, we make a simple investigation on the convergence of central deflection and central bending moment M_x through the methods of knot insertion and order elevation in Fig. 7. The same certain number of knots were inserted into knot vectors in the two patches and the same intervals were kept between any two adjacent knots but with different value of knots. It is observed that better convergence can be obtained with the higher order of basis functions. Exact thin plate deflection on central point of this problem can be denoted as $w = 0.0040624\frac{q_0 a^4}{D_0}$ and the result of convergence here is given by $w = 0.0040970\frac{q_0 a^4}{D_0}$. The transverse displacement is 0.84% bigger than analytical solution and almost equals to the result from single patch. We note that the stabilization parameter β has negligible effect on the solutions when the value is chosen within the range from 1×10^5 to 1×10^{16} for this problem. The parameter here and in the following three examples are all set to be 1×10^8 empirically, and details of the states can be found in Embar et al. (2010).

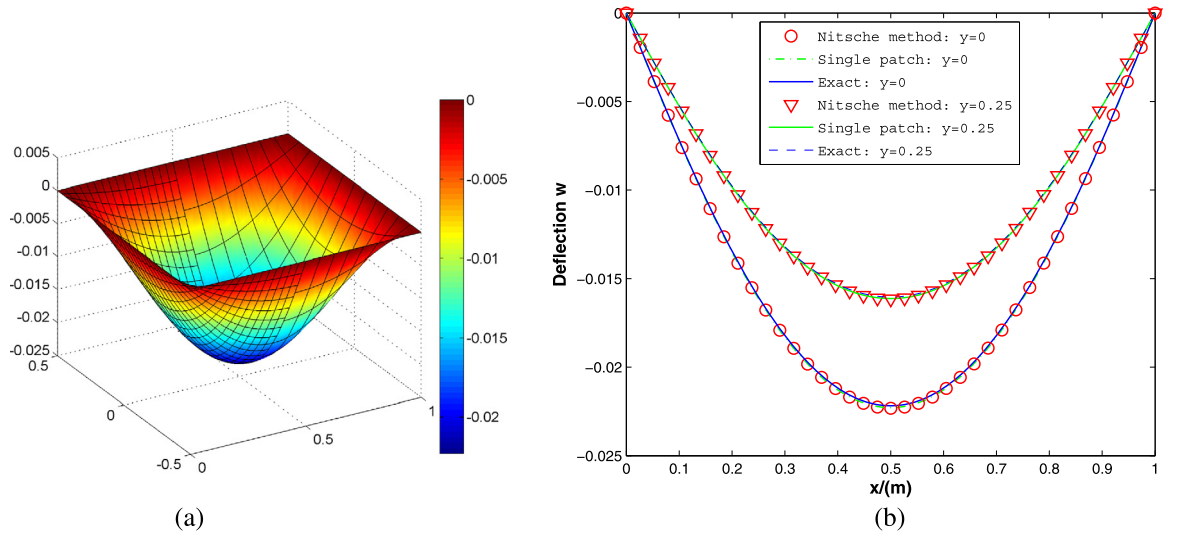

Fig. 4. Simply supported square plate under uniform load: deflection w. (a) The deflection on both two domains and (b) in comparison with the solution on single patch and the exact solution along the lines of $y = 0$ and $y = 0.25a$.

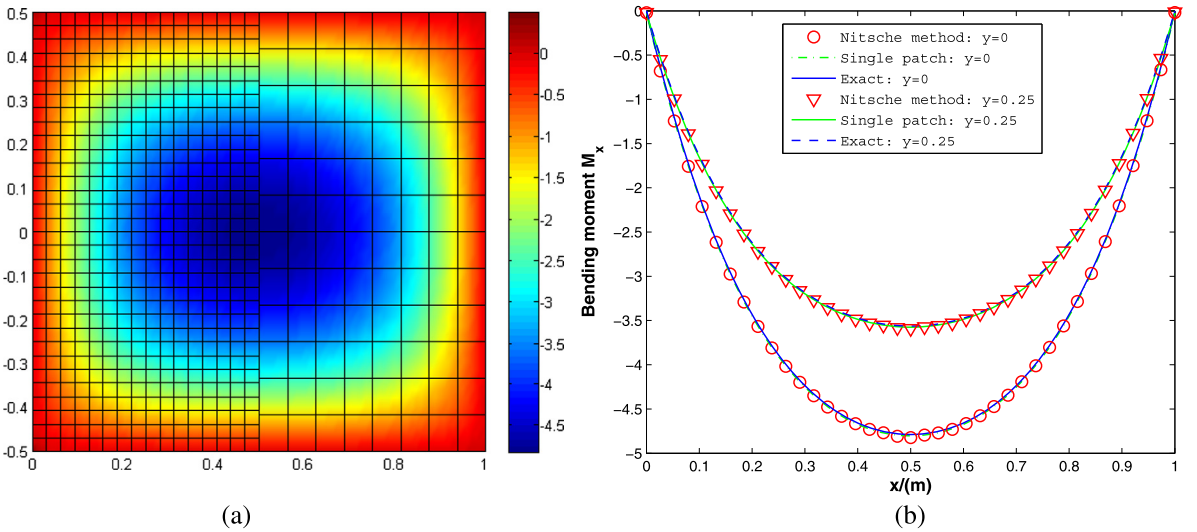

Fig. 5. Simply supported square plate under uniform load: bending moment M_x. (a) The bending moment M_x on both two domains and (b) in comparison with the solution on single patch and the exact solution along the lines of $y = 0$ and $y = 0.25a$.

6.2. Simply supported square plate under sinusoidal distributed load

In this problem, we use the same square model as in the above example but substituting sinusoidal load for uniform load. The coordinate system should also be made a few small changes. We translate the x-axis in Fig. 3(a) to coincide with the bottom side of the square plate. The thickness and length of side of the plate are assumed to be $t = 0.01$ m, and $a = 1$ m, respectively. The distributed load over the surface of plate is given by:

$$q = q_0 \sin\frac{\pi x}{a} \sin\frac{\pi y}{b}$$

where $q_0 = -10$ N. With simply supported boundary conditions on all sides, the exact deflection w of this problem is expressed as Timoshenko et al. (1959):

$$w = \frac{q_0}{\pi^4 D_0 \left(\frac{1}{a^2} + \frac{1}{b^2}\right)^2} \sin\frac{\pi x}{a} \sin\frac{\pi y}{b} \tag{34}$$

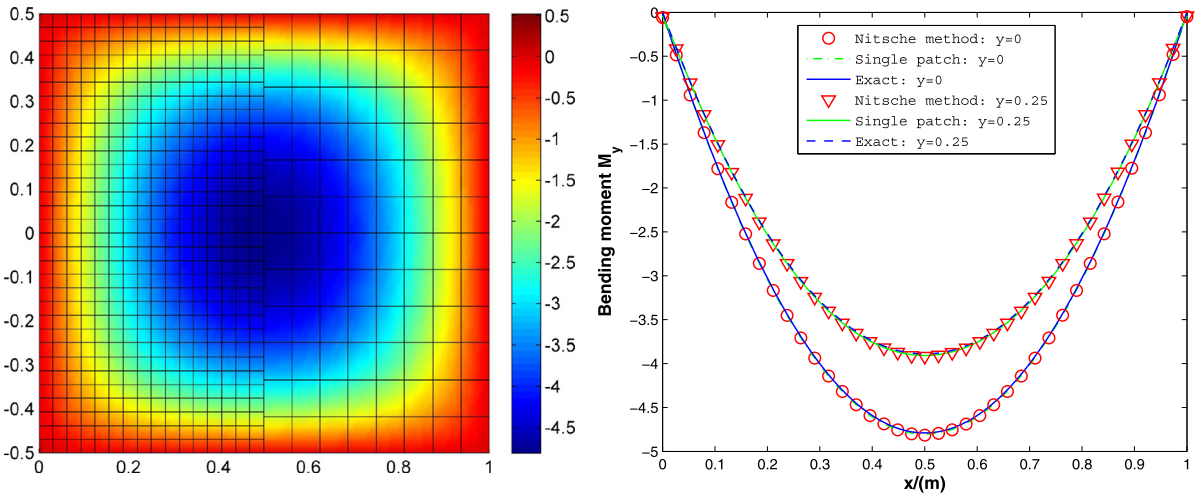

Fig. 6. Simply supported square plate under uniform load: bending moment M_y. (a) The bending moment M_y on both two domains and (b) in comparison with the solution on single patch and the exact solution along the lines of $y = 0$ and $y = 0.25a$.

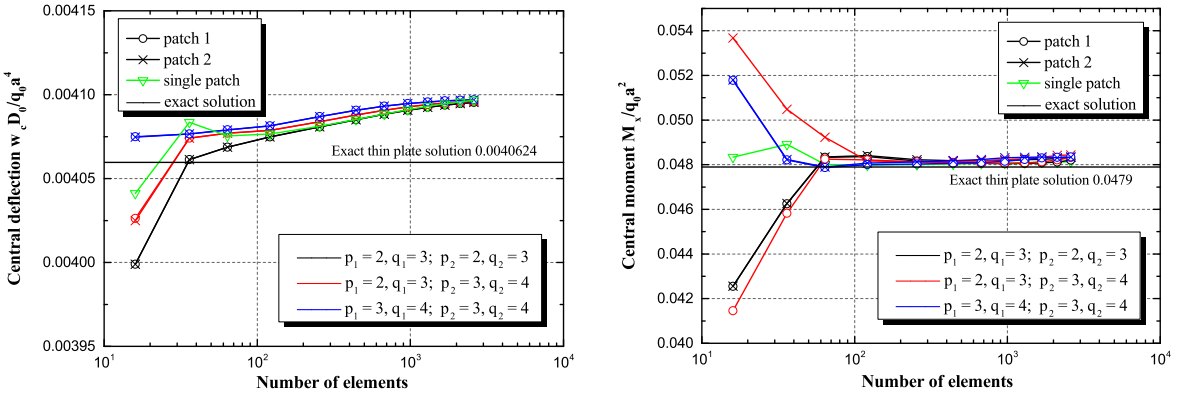

Fig. 7. Simply supported square plate under uniform load: the convergence of central deflection and moment. (a) The convergence of central deflection w and (b) the convergence of central bending moment M_x.

where $a = b$ for square plate. The plate is constructed with two NURBS patches with the physical domains denoted by $\Omega^1 = \{0 \le x < a/2, 0 \le y \le b\}$ and $\Omega^2 = \{a/2 < x \le a, 0 \le y \le b\}$. Two different discretizations are implemented in both patches: 16×16 elements and polynomial degrees $p_1 = 2$, $q_1 = 3$ for patch 1, 11×11 elements and polynomial degrees $p_2 = 3$, $q_2 = 4$ for patch 2 see Fig. 8(a). Fig. 8(b) shows the transverse displacement of the plate. Absolute error of deflection on the whole domains is plotted in Fig. 8(c) with exact solution as a reference. The deflection and its absolute error are continuous across the interface as post processing figures show. Fig. 9 describes the convergence of central deflection under different order circumstances. The deflection in Nitsche method converge to $0.0025840\frac{q_0}{D_0}$, which is 0.68% larger than the analytical solution $0.0025665\frac{q_0}{D_0}$.

6.3. Clamped circle plate subjected to uniform load

We investigate the uniformly loaded circle plate with radius $a = 1$ m in this section. Thickness of the plate $t = 0.01$ m and uniform load $q_0 = -10$ N. If outer edge is fixed, the exact thin plate solution in terms of deflection is given by Timoshenko et al. (1959):

$$w = \frac{q_0}{64D_0}(a^2 - r^2)^2 \tag{35}$$

where r is the radial distance from the center of circle plate.

We model the plate with two symmetrical patches and build non-conforming mesh, where left patch is discretized by 7×9 elements with polynomial degrees $p_1 = 3$, $q_1 = 4$ and right patch is discretized by 7×7 elements with polynomial

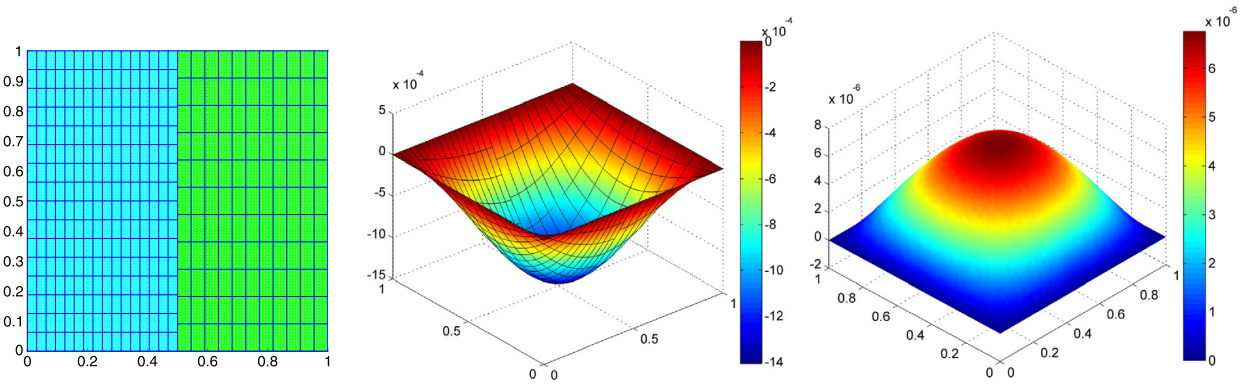

(a) Non-conforming mesh (b) Deflection w (c) Absolute error

Fig. 8. Simply supported square plate under sinusoidal load. Patch 1 is built with 16×16 elements and polynomial degrees $p_1 = 2$, $q_1 = 3$; patch 2 is built with 11×11 elements and polynomial degrees $p_2 = 3$, $q_2 = 4$. (a) Non-conforming mesh, (b) deflection and (c) absolute error of deflection.

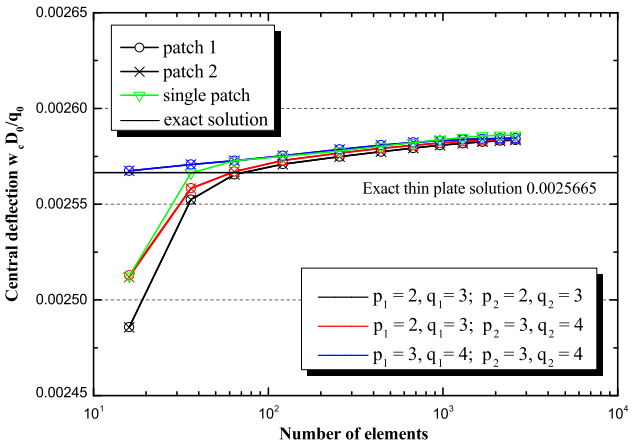

Fig. 9. Simply supported square plate under sinusoidal load: the convergence of central deflection.

degrees $p_2 = 4$, $q_2 = 5$, see Fig. 10(a). Here circle dots denote the control points of corresponding NURBS patch and blue lines express the parameter lines forming the elements. Fig. 10(b) shows the deflection of the middle plane of the plate. The absolute error can be obtained as given in Fig. 10(c) when compared to the analytical solution computed by Eq. (35). The convergence of central deflection of the circle plate is studied with different order in NURBS patches from Fig. 11. The exact thin plate solution of deflection $0.015625\frac{q_0}{D_0}$ is 0.68% smaller than the result of convergence $0.015732\frac{q_0}{D_0}$ calculated by Nitsche method under Mindlin theory.

6.4. Clamped square plate under a suitable body load

In this section, we consider a benchmark problem to study the convergence of the method. This problem consists of a unit square plate $\Omega \in [-1, 1]^2$ subjected to a body load $\mathbf{f}$ with all sides clamped, in which an analytical solution is explicitly known (Chinosi and Lovadina, 1995). The load $\mathbf{f}$ is the transverse load applied to the plate and can be expressed as:

$$\mathbf{f} = (0, 0, t^2 f(x, y)) \tag{36}$$

where

$$f(x, y) = \frac{E}{12(1-\nu^2)}[12y(y-1)(5x^2-5x+1)(2y^2(y-1)^2 + x(x-1)(5y^2-5y+1)) + 12x(x-1)(5y^2-5y+1)(2x^2(x-1)^2 + y(y-1)(5x^2-5x+1))] \tag{37}$$

The analytical solution of rotations and deflection is given by:

$$\theta_x(x, y) = x^3(x-1)^3y^2(y-1)^2(2y-1) \tag{38}$$

$$\theta_y(x, y) = y^3(y-1)^3x^2(x-1)^2(2x-1) \tag{39}$$

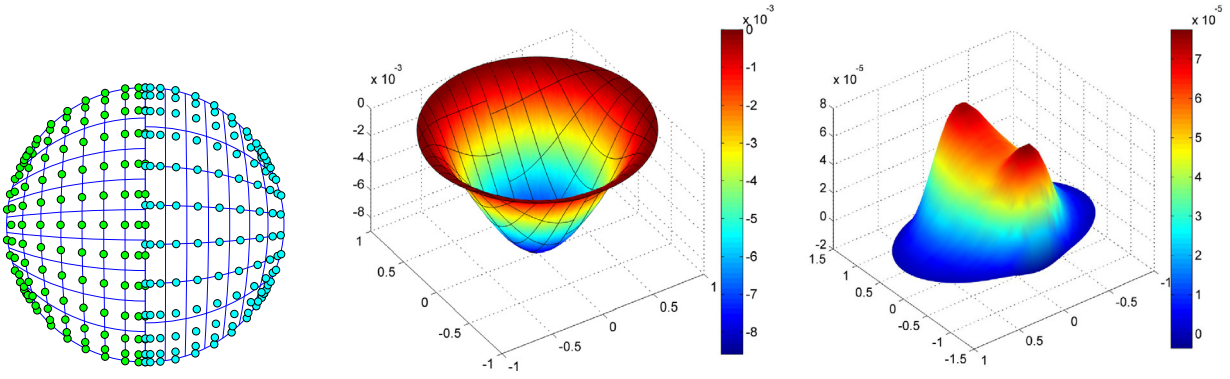

(a) Non-conforming mesh and control points (b) Deflection (c) Absolute error

Fig. 10. Clamped circle plate subjected to uniform load. Patch 1 is built with 7×9 elements and polynomial degrees $p_1 = 3$, $q_1 = 4$; patch 2 is built with 7×7 elements and polynomial degrees $p_2 = 4$, $q_2 = 5$. (a) Two patch with non-conforming mesh, (b) deflection and (c) absolute error of deflection. (For interpretation of the references to color in this figure, the reader is referred to the web version of this article.)

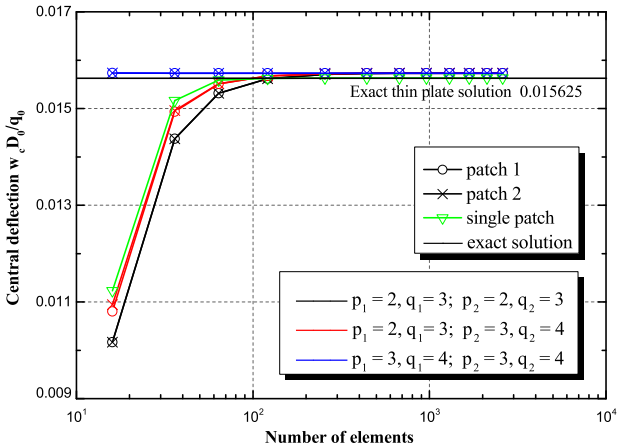

Fig. 11. Clamped circle plate subjected to uniform load: the convergence of central deflection.

$$w(x,y) = \frac{1}{3}x^3(x-1)^3y^3(y-1)^3 - \frac{2t^2}{5(1-\nu)}[y^3(y-1)^3x(x-1)(5x^2-5x+1) + x^3(x-1)^3y(y-1)(5y^2-5y+1)] \tag{40}$$

Based on the displacements, the bending moments and shear forces were deduced (Kiendl et al., 2015):

$$M_x = \frac{Et^3}{6(1-\nu^2)}[y^3(y-1)^3(x-x^2)(5x^2-5x+1) + \nu(x^3(x-1)^3(y-y^2)(5y^2-5y+1))] \tag{41}$$

$$Q_x = -\frac{Et^3}{6(1-\nu^2)}[y^3(y-1)^3(20x^3-30x^2+12x-1) + 3y(y-1)(5y^2-5y+1)x^2(x-1)^2(2x-1)] \tag{42}$$

The formulations of bending moment M_y, twist moment M_{xy} and shear force Q_y can be found in Kiendl et al. (2015), Beirão da Veiga et al. (2015). The material parameters and thickness are $E = 10.92 \times 10^6$, $\nu = 0.3$ and $t = 0.1$ m. The convergence rate of Nitsche method in L_2-norm is studied here with the comparison to that from the isogeometric analysis on single patch, using different level of refinement. The relative L_2-norm approximation error can be defined as:

$$E_\psi = \frac{\|\psi_{ex} - \psi_h\|_\Omega^{L_2}}{\|\psi_{ex}\|_\Omega^{L_2}} \tag{43}$$

where ψ represents unknown variables, ψ_{ex} the exact solution and ψ_h expresses numerical solution with the discretization of element size h. The k-refinement strategy in isogeometric analysis was used to refine the domains to ensure C^{p-1}

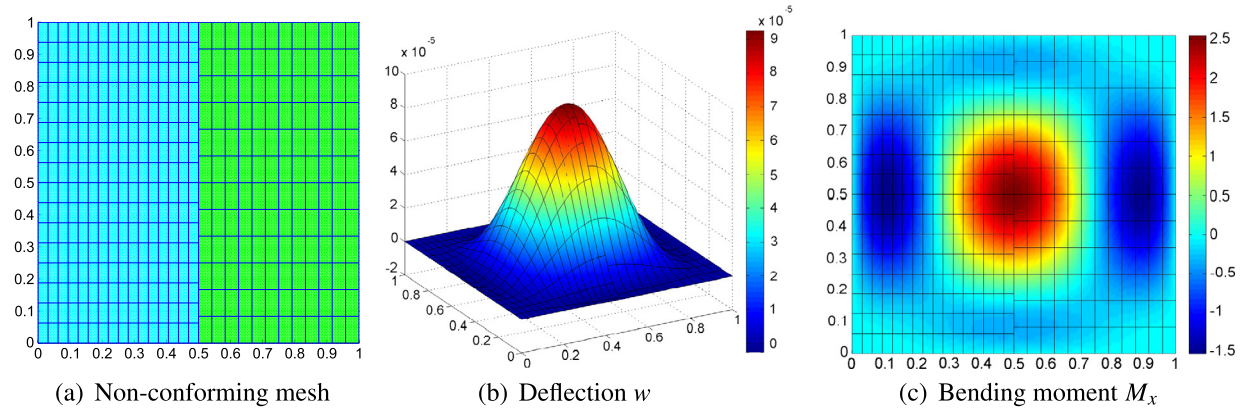

(a) Non-conforming mesh (b) Deflection w (c) Bending moment M_x

Fig. 12. Clamped unit square plate under a suitable body load. Patch 1 is built with 16×16 elements and biquadratic polynomial degrees; patch 2 is built with 12×12 elements and bicubic polynomial degrees. (a) Non-conforming mesh, (b) deflection and (c) bending moment M_x.

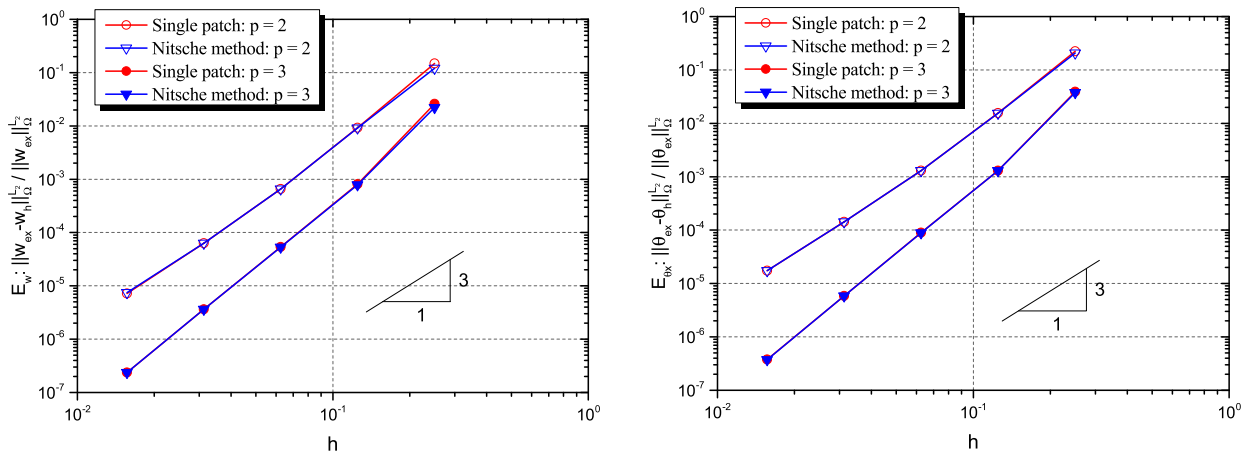

(a) Convergence rate of deflection w (b) Convergence rate of rotation θ_x

Fig. 13. Clamped unit square plate under a body load: the relative error in L_2 norm. (a) Deflection and (b) rotation θ_x.

continuities across inner-elements, as a result of the existence of marginal benefits with higher-continuous basis functions (Collier et al., 2014).

We present the post-processing images of deflection w and bending moment M_x with the discretization 16×16 elements and biquadratic degrees for patch 1, 12×12 elements and bicubic degrees for patch 2 as shown in Fig. 12. Then the convergence of deflection and rotation θ_x is studied with the same uniformly refined strategy for two patches. A cubic convergence rate of relative error in the L_2-norm for the case of $p = 2$ and a quartic convergence rate for $p = 3$ can be obtained as shown in Fig. 13(a) and 13(b) plotted in a unified *log–log* scale, where p represents the equal degrees in two parameter directions of a patch. In addition, optimal rates of convergence of bending moments M_x and shear force Q_x can be obtained as shown in Fig. 14(a) and 14(b). We can find that the convergence rate of the Nitsche method for non-conforming problems keeps consistent with the results that from single patch.

6.5. Uniformly loaded cantilever plate

In this example, a cantilever plate under uniformly distributed load is investigated. We assume that bottom boundary of the plate is clamped, uniform load $q_0 = -10$ N, and thickness $t = 20$ mm. The material properties Young modulus $E = 1 \times 10^{10}$, Poisson ratio $\nu = 0.3$ and stabilization parameter is chosen as 1×10^{12}. Dimension and boundary conditions of cantilever plate are depicted in Fig. 15. The plate is modeled by four patches and the discretizations are listed as follows: 12×12 elements for patch 1; 9×9 elements for patch 2; 12×12 elements for patch 3; and 9×9 elements for patch 4. All patches are built with biquadratic NURBS basis functions and the mesh is non-matching along the interfaces. Fig. 16(a) shows the transverse displacement of plate in solid model analyzed by commercial software *ABAQUS* where up to 76853 hexahedral elements are built, and the maximum deflection here is 7.570×10^{-4} mm. The deflection pattern of the plate based isogeometric method is plotted in Fig. 16(b) and maximum value is 7.466×10^{-4} mm. Generally, in isogeometric analysis, conforming mesh needs to be built along the four common boundaries, which compels us to do complex and time

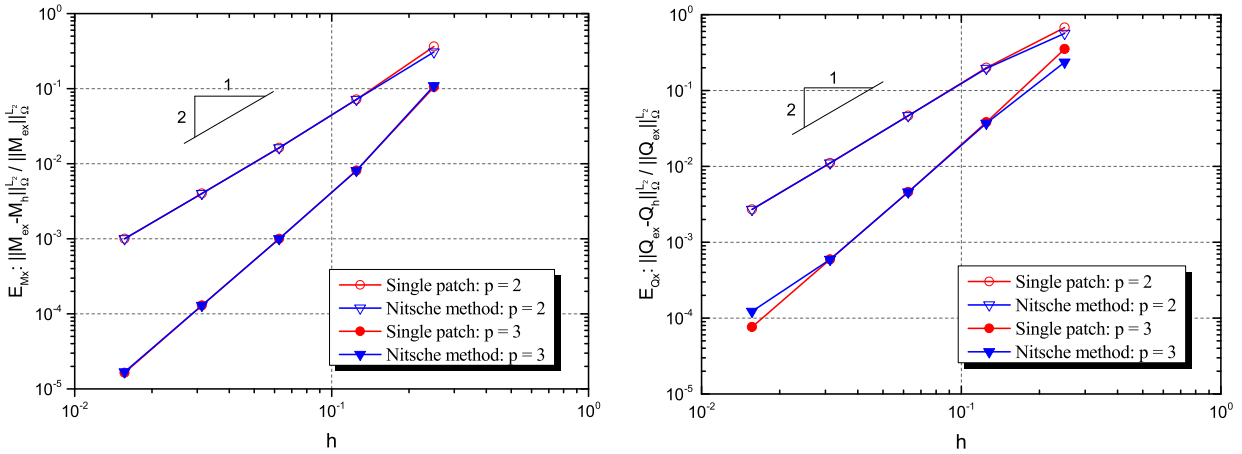

(a) Convergence rate of bending moment M_x (b) Convergence rate of shear force Q_x

Fig. 14. Clamped unit square plate under a body load: the relative error in L_2 norm. (a) Bending moment M_x and (b) shear force Q_x.

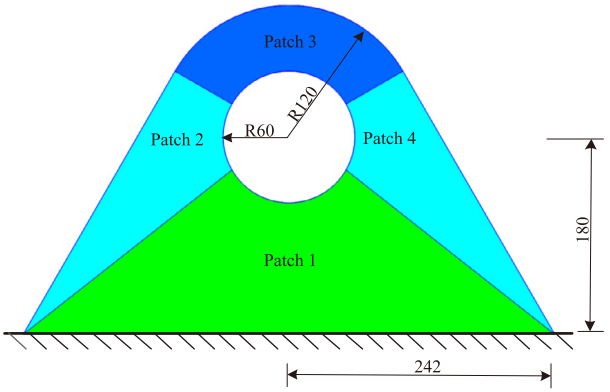

Fig. 15. Cantilever plate: geometry, dimensions and boundary conditions. Units: mm.

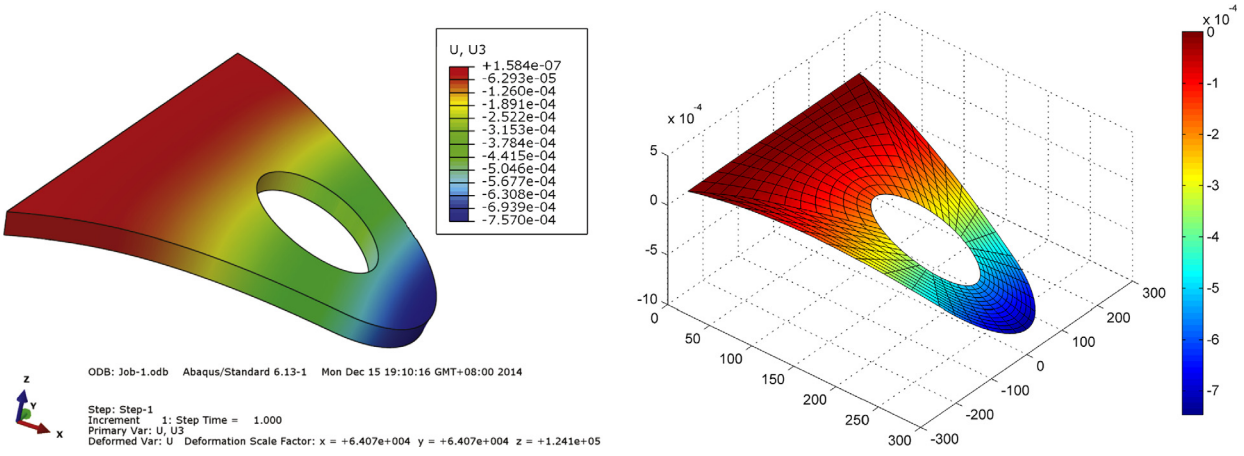

(a) FEA (b) IGA

Fig. 16. The deflection of the cantilever plate: (a) FEA in commercial software *ABAQUS* and (b) IGA with Nitsche method.

consuming work including knot insertion and order elevation. More complex models, especially those utilized in big industries like autos and aerospace and so on, are almost surely to involve elements trimmed by different patches' boundaries, which need to be treated differently and are under investigation now based on the work presented here.

7. Conclusion

In this work, we have adopted the Nitsche method to develop the NURBS-based isogeometric analysis of multi-patch plates, which are discretized into non-conforming mesh along the interfaces. The presented method relieves us from the complicated coupling operation that often occurs in isogeometric method in order to obtain conforming mesh, which is time-saving and straightforward. The Reissner–Mindlin plate theory has been employed to analyze some classical plate models and a complex cantilever plate model. Analytical solutions in Kirchhoff hypothesis, numerical solutions of single-patch models in Mindlin theory and results from the *ABAQUS* hexahedral element have been used to make comparison. In the comparison with different variables in classical thin plate, we find that solutions in Mindlin theory are slightly different with that in Kirchhoff theory because of the augmentation of shear deformation terms to the total potential energy functional. Meanwhile, for the same model, the results obtained from non-conforming situations coincide with that from single patch in Mindlin theory under the framework of isogeometric analysis. Optimal convergence rate can be achieved with Nitsche method. The results in different examples show the robustness, accuracy and high-efficiency convergence of Nitsche method in conjunction with isogeometric method.

We investigated the numerical examples with single-patch, two-patch and four-patch plates, and limited the contributions to the linear elastic problems. More complex geometries with non-conforming multi-patches and trimming patches are frequently designed in practical use. Thus, future studies will focus on the complex geometries built with non-conforming and trimming multi-patches, and the extension of this method to non-linear problems.

Acknowledgements

The authors would like to acknowledge the support by the Natural Science Foundation of China (Project No. 51305016).

References

Annavarapu, C., Hautefeuille, M., Dolbow, J.E., 2012. A robust Nitsches formulation for interface problems. Comput. Methods Appl. Mech. Eng. 225, 44–54.
Apostolatos, A., Schmidt, R., Wüchner, R., Bletzinger, K.-U., 2014. A Nitsche-type formulation and comparison of the most common domain decomposition methods in isogeometric analysis. Int. J. Numer. Methods Eng. 97 (7), 473–504.
Auricchio, F., Calabro, F., Hughes, T., Reali, A., Sangalli, G., 2012. A simple algorithm for obtaining nearly optimal quadrature rules for NURBS-based isogeometric analysis. Comput. Methods Appl. Mech. Eng. 249, 15–27.
Bazilevs, Y., Calo, V., Hughes, T., Zhang, Y., 2008. Isogeometric fluid-structure interaction: theory, algorithms, and computations. Comput. Mech. 43 (1), 3–37.
Bazilevs, Y., Calo, V., Zhang, Y., Hughes, T.J., 2006. Isogeometric fluid-structure interaction analysis with applications to arterial blood flow. Comput. Mech. 38 (4–5), 310–322.
Beirão da Veiga, L., Buffa, A., Lovadina, C., Martinelli, M., Sangalli, G., 2012. An isogeometric method for the Reissner–Mindlin plate bending problem. Comput. Methods Appl. Mech. Eng. 209, 45–53.
Beirão da Veiga, L., Hughes, T., Kiendl, J., Lovadina, C., Niiranen, J., Reali, A., Speleers, H., 2015. A locking-free model for Reissner–Mindlin plates: analysis and isogeometric implementation via NURBS and triangular NURPS. Preprint.
Benson, D., Bazilevs, Y., Hsu, M.-C., Hughes, T., 2011. A large deformation, rotation-free, isogeometric shell. Comput. Methods Appl. Mech. Eng. 200 (13), 1367–1378.
Brunero, F., Pavarino, L.F., Pechstein, C., 2012. Discontinuous Galerkin methods for isogeometric analysis. Ph.D. thesis, Masters thesis. Universita degli Studi di Milano.
Buffa, A., Sangalli, G., Vázquez, R., 2010. Isogeometric analysis in electromagnetics: B-splines approximation. Comput. Methods Appl. Mech. Eng. 199 (17), 1143–1152.
Chinosi, C., Lovadina, C., 1995. Numerical analysis of some mixed finite element methods for Reissner–Mindlin plates. Comput. Mech. 16 (1), 36–44.
Cockburn, B., Karniadakis, G.E., Shu, C.-W., 2000. Discontinuous Galerkin methods: theory, computation and applications. Lect. Notes Comput. Sci. Eng. 11, 3–53.
Collier, N., Dalcin, L., Calo, V., 2014. On the computational efficiency of isogeometric methods for smooth elliptic problems using direct solvers. Int. J. Numer. Methods Eng. 100 (8), 620–632.
Cottrell, J.A., Hughes, T.J., Bazilevs, Y., 2009. Isogeometric Analysis: Toward Integration of CAD and FEA. John Wiley & Sons.
Cottrell, J., Hughes, T., Reali, A., 2007. Studies of refinement and continuity in isogeometric structural analysis. Comput. Methods Appl. Mech. Eng. 196 (41), 4160–4183.
Cottrell, J., Reali, A., Bazilevs, Y., Hughes, T., 2006. Isogeometric analysis of structural vibrations. Comput. Methods Appl. Mech. Eng. 195 (41), 5257–5296.
Deng, J., Chen, F., Li, X., Hu, C., Tong, W., Yang, Z., Feng, Y., 2008. Polynomial splines over hierarchical t-meshes. Graph. Models 70 (4), 76–86.
Dokken, T., Lyche, T., Pettersen, K.F., 2013. Polynomial splines over locally refined box-partitions. Comput. Aided Geom. Des. 30 (3), 331–356.
Dolbow, J., Harari, I., 2009. An efficient finite element method for embedded interface problems. Int. J. Numer. Methods Eng. 78 (2), 229–252.
Embar, A., Dolbow, J., Harari, I., 2010. Imposing Dirichlet boundary conditions with Nitsche's method and spline-based finite elements. Int. J. Numer. Methods Eng. 83 (7), 877–898.
Gómez, H., Calo, V.M., Bazilevs, Y., Hughes, T.J., 2008. Isogeometric analysis of the Cahn–Hilliard phase-field model. Comput. Methods Appl. Mech. Eng. 197 (49), 4333–4352.
Guo, Y., Ruess, M., 2015. Nitsches method for a coupling of isogeometric thin shells and blended shell structures. Comput. Methods Appl. Mech. Eng. 284, 881–905.
Hesch, C., Betsch, P., 2012. Isogeometric analysis and domain decomposition methods. Comput. Methods Appl. Mech. Eng. 213, 104–112.
Hughes, T.J., Cottrell, J.A., Bazilevs, Y., 2005. Isogeometric analysis: cad, finite elements, NURBS, exact geometry and mesh refinement. Comput. Methods Appl. Mech. Eng. 194 (39), 4135–4195.

Hughes, T.J., Reali, A., Sangalli, G., 2010. Efficient quadrature for NURBS-based isogeometric analysis. Comput. Methods Appl. Mech. Eng. 199 (5), 301–313.
Kiendl, J., Auricchio, F., da Veiga, L.B., Lovadina, C., Reali, A., 2015. Isogeometric collocation methods for the Reissner–Mindlin plate problem. Comput. Methods Appl. Mech. Eng. 284, 489–507.
Kiendl, J., Bletzinger, K.-U., Linhard, J., Wüchner, R., 2009. Isogeometric shell analysis with Kirchhoff–Love elements. Comput. Methods Appl. Mech. Eng. 198 (49), 3902–3914.
Lacour, C., Maday, Y., 1997. Two different approaches for matching nonconforming grids: the mortar element method and the feti method. BIT Numer. Math. 37 (3), 720–738.
Marini, L.D., 2008. Discontinuous Galerkin Elements for Reissner–Mindlin Plates. Springer.
Mergheim, J., Kuhl, E., Steinmann, P., 2004. A hybrid discontinuous Galerkin/interface method for the computational modelling of failure. Commun. Numer. Methods Eng. 20 (7), 511–519.
Moro, F., Alotto, P., Guarnieri, M., Stella, A., 2014. Domain decomposition with the mortar cell method. Int. J. Numer. Model. 27 (3), 461–471.
Nguyen, V.P., Kerfriden, P., Brino, M., Bordas, S.P., Bonisoli, E., 2014. Nitsches method for two and three dimensional NURBS patch coupling. Comput. Mech. 53 (6), 1163–1182.
Nitsche, J., 1971. Über ein variationsprinzip zur lösung von Dirichlet-problemen bei verwendung von teilräumen, die keinen randbedingungen unterworfen sind. In: Abh. Math. Semin. Univ. Hamb., vol. 36. Springer, pp. 9–15.
Noels, L., Radovitzky, R., 2008. A new discontinuous Galerkin method for Kirchhoff–Love shells. Comput. Methods Appl. Mech. Eng. 197 (33), 2901–2929.
Piegl, L., Tiller, W., 1997. The NURBS Book, 2nd ed.
Quek, S., Liu, G., 2003. Finite Element Method: A Practical Course. Butterworth–Heinemann.
Sanders, J.D., Laursen, T.A., Puso, M.A., 2012. A Nitsche embedded mesh method. Comput. Mech. 49 (2), 243–257.
Schillinger, D., Hossain, S.J., Hughes, T.J., 2014. Reduced Bézier element quadrature rules for quadratic and cubic splines in isogeometric analysis. Comput. Methods Appl. Mech. Eng. 277, 1–45.
Sederberg, T.W., Finnigan, G.T., Li, X., Lin, H., Ipson, H., 2008. Watertight trimmed NURBS. ACM Trans. Graph. 27 (3), 79.
Sederberg, T.W., Zheng, J., Bakenov, A., Nasri, A., 2003. T-Splines and t-NURCCs. ACM Trans. Graph., vol. 22. ACM, pp. 477–484.
Shojaee, S., Valizadeh, N., 2012. NURBS-based isogeometric analysis for thin plate problems. Struct. Eng. Mech. 41 (5), 617–632.
Thai, C.H., Nguyen-Xuan, H., Nguyen-Thanh, N., Le, T.-H., Nguyen-Thoi, T., Rabczuk, T., 2012. Static, free vibration, and buckling analysis of laminated composite Reissner–Mindlin plates using NURBS-based isogeometric approach. Int. J. Numer. Methods Eng. 91 (6), 571–603.
Timoshenko, S., Woinowsky-Krieger, S., Woinowsky-Krieger, S., 1959. Theory of Plates and Shells, vol. 2. McGraw–Hill, New York.
Toselli, A., Widlund, O., 2005. Domain Decomposition Methods: Algorithms and Theory, vol. 3. Springer.
Ventsel, E., Krauthammer, T., 2001. Thin Plates and Shells: Theory, Analysis, and Applications. CRC Press.
Wang, D., Xuan, J., 2010. An improved NURBS-based isogeometric analysis with enhanced treatment of essential boundary conditions. Comput. Methods Appl. Mech. Eng. 199 (37), 2425–2436.
Zhu, J., Taylor, Z., Zienkiewicz, O., 2005. The Finite Element Method: Its Basis and Fundamentals.
Zienkiewicz, O.C., Taylor, R.L., 2005. The Finite Element Method for Solid and Structural Mechanics. Butterworth–Heinemann.